Magnetic and Thermodynamic Properties of the Collective Paramagnet–Spin Liquid Pyrochlore $Tb_2Ti_2O_7$

M. J. P. Gingras[1,2], B. C. den Hertog[2], M. Faucher[3], J.S. Gardner[4,†], L.J. Chang[5], B.D. Gaulin[1,4], N.P. Raju[6,‡] J.E. Greedan[6]

[1]*Canadian Institute for Advanced Research*

[2]*Department of Physics, University of Waterloo, Waterloo, Ontario, N2L 3G1, Canada*

[3]*Laboratoire SPMS, Ecole Centrale de Paris, 92295, Chatenay-Malabry, Cedex, France*

[4]*Department of Physics and Astronomy, McMaster University, Hamilton, Ontario, L8S 4M1, Canada*

[5]*Institute of Physics, Academia Sinica, Taipei, Taiwan, Republic of China*

[6]*Brockhouse Institute for Materials Research and Department of Chemistry, McMaster University, Hamilton, Ontario, L8S 4M1, Canada*

(February 1, 2008)

In a recent letter [Phys. Rev. Lett. **82**, 1012 (1999)] it was found that the Tb^{3+} magnetic moments in the $Tb_2Ti_2O_7$ pyrochlore lattice of corner-sharing tetrahedra remain in a *collective paramagnetic* state down to 70mK. In this paper we present results from d.c. magnetic susceptibility, specific heat data, inelastic neutron scattering measurements, and crystal field calculations that strongly suggest that (1) the Tb^{3+} ions in $Tb_2Ti_2O_7$ possess a moment of approximatively $5\mu_B$, and (2) the ground state $g-$tensor is extremely anisotropic below a temperature of $O(10^0)$K, with Ising-like Tb^{3+} magnetic moments confined to point along a local cubic $\langle 111\rangle$ diagonal (e.g. towards the middle of the tetrahedron). Such a very large easy-axis Ising like anisotropy along a $\langle 111\rangle$ direction dramatically reduces the frustration otherwise present in a Heisenberg pyrochlore antiferromagnet. The results presented herein underpin the conceptual difficulty in understanding the microscopic mechanism(s) responsible for $Tb_2Ti_2O_7$ failing to develop long-range order at a temperature of the order of the paramagnetic Curie-Weiss temperature $\theta_{CW} \approx -10^1$K. We suggest that dipolar interactions and extra perturbative exchange coupling(s) beyond nearest-neighbors may be responsible for the lack of ordering of $Tb_2Ti_2O_7$.

I. INTRODUCTION

In magnetic systems, competition between magnetic interactions, combined with certain local lattice symmetries involving triangles, give rise to the notion of *geometric frustration* [1,2]. Geometrically frustrated antiferromagnets are currently attracting much interest within the condensed matter community [2,3]. The main reason for this interest is that geometric frustration can cause sufficiently large zero-temperature quantum spin fluctuations as to drive a system into novel types of intrinsically quantum mechanical magnetic ground states with no classical equivalent [3–5].

Among three-dimensional systems, the pyrochlore lattice of corner-sharing tetrahedra (see Fig. 1) with antiferromagnetic nearest-neighbor exchange interaction is particularly interesting. For this system, theory [6–8] and Monte Carlo simulations [8,9] show that for classical Heisenberg magnetic moments interacting with a nearest-neighbor antiferromagnetic coupling, there is no transition to long-range magnetic order at finite temperature. This is unlike the two-dimensional kagomé lattice antiferromagnet [8,10,11] where a thermally-driven order-by-disorder of spin nematic order occurs. Villain coined the name *"collective paramagnetic"* to describe the *classical state* of the pyrochlore lattice at low temperatures [6].

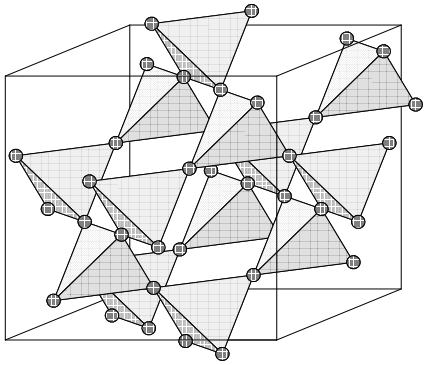

FIG. 1. Pyrochlore lattice of corner-sharing tetrahedra. The magnetic moments occupy the corners of the tetrahedra.

Because of their low propensity to order even for classical spins, antiferromagnetic materials based on a pyrochlore lattice appear to be excellent systems in which to seek exotic quantum mechanical ground states. For example, numerical calculations suggest that the $S = 1/2$ pyrochlore Heisenberg antiferromagnet may be fully quantum disordered, giving rise to a state that is commonly referred to as *"spin liquid"* [5]. Both terms "collective-paramagnet" and "spin liquid" are meant to

emphasize that despite such a system remaining in a paramagnetic phase down to absolute zero temperature, the properties of such a state involve very strong and nontrivial short-range spin correlations, analogous to the nontrivial position-position correlations present in an ordinary atomic or molecular fluid.

A number of experimental studies on insulating pyrochlore materials have been reported in the past ten years. Interestingly, it has been found that such systems do not typically form such a spin liquid state that remains paramagnetic down to zero temperature. Most often, these systems either display long-range antiferromagnetic order; such as FeF_3 [12], $Gd_2Ti_2O_7$ [13,14], $ZnFe_2O_4$ [15,16], and $ZnCr_2O_4$ [16,17], or enter a spin-glass-like state below some nonzero spin-freezing temperature as exhibited by $Y_2Mo_2O_7$ [18–20], $Tb_2Mo_2O_7$ [18,21], $Y_2Mn_2O_7$ [22], as well as the disordered $CsNiCrF_6$ pyrochlore [23].

Recently, several studies of the pyrochlore rare-earth titanates, $R_2Ti_2O_7$, have been published [24]. In these compounds, the trivalent rare earth ions, R^{3+}, occupy the 16d sites of the $Fd\bar{3}m$ space and form a pyrochlore lattice (Fig. 1). The behaviors displayed in this family of pyrochlores are much varied indeed. $Gd_2Ti_2O_7$ develops true long-range order at a critical temperature of about 1K [13,14]. $Tm_2Ti_2O_7$ possesses a trivial nonmagnetic (i.e. spin singlet) ground state separated by an energy gap of about 120 K to the next crystal field level [25]. $Ho_2Ti_2O_7$ is well described by an Ising doublet [26]. In that system, it was originally argued that the nearest-neighbor exchange interaction is weakly ferromagnetic [26], and that the strong Ising-like single ion anisotropy along (111) directions frustrates the development of long range ferromagnetic order [26–33]. This material also exhibits low temperature spin dynamics reminiscent of Pauling's "ice model" [34], an equivalence proposed by Harris and co-workers [26,31–33]. Recently, it has been found that $Dy_2Ti_2O_7$ [35] is also a very good example of "spin ice" [26,31–33], and that the application of a magnetic field can restore much of the ground-state entropy and drive magnetic phase transitions. Most recently, den Hertog and Gingras have argued that the spin ice physics in both $Ho_2Ti_2O_7$ and $Dy_2Ti_2O_7$ is not driven by nearest-neighbor ferromagnetic exchange, but is rather due to the *long-range* $1/r^3$ nature of magnetic dipole-dipole interactions [29,30].

In contrast to the long-range ordered or spin glass states mentioned above, strong evidence for collective paramagnetism, or spin liquid behavior, was recently observed in the insulating pyrochlore $Tb_2Ti_2O_7$ [36,37]. It was found using neutron scattering and muon spin relaxation methods that this material remains paramagnetic down to (at least) 70 mK despite the fact that the paramagnetic Curie-Weiss temperature, $\theta_{\rm CW}$, is -19 K, and that short-range antiferromagnetic correlations begin to develop at ~ 50 K. At first sight, one could argue that it is "pleasing" to have found at last the spin liquid state anticipated by theory for a highly frustrated pyrochlore antiferromagnet [6–9]. However, the situation for $Tb_2Ti_2O_7$ is not as simple as it might naively appear.

In $Tb_2Ti_2O_7$ the Tb^{3+} ions have a partially filled ${}^7F_6$ shell, and one most first understand their crystal field level scheme and, in particular, the nature of the single-ion magnetic ground state before constructing a correct effective spin-spin Hamiltonian for $Tb_2Ti_2O_7$. Indeed, we show below that crystal field anisotropy renders the description of $Tb_2Ti_2O_7$ in terms of an isotropic Heisenberg antiferromagnetic model completely inappropriate.

If one neglects the axial oxygen distortion around the Tb^{3+} sites, and assumes that the local environment of the Tb^{3+} is perfectly cubic, one would expect, based on point charge calculations, that the ground state of both Tb^{3+} and Tm^{3+} should either be a singlet or a nonmagnetic doublet [38]. For example, as mentioned above, experimental evidence for a nonmagnetic singlet ground state has been found in $Tm_2Ti_2O_7$ [25]. Based on this naive picture, one can see that the experimental evidence of a moment for Tb^{3+} in $Tb_2Ti_2O_7$ is therefore a nontrivial issue that needs to be understood.

A simple possibility is that corrections beyond the point-charge approximation and/or the known axial oxygen distortions around each of the 16d sites cause the Tb^{3+} cations to acquire a permanent magnetic moment. Another and more interesting possibility, is that the moment on the Tb^{3+} site in $Tb_2Ti_2O_7$ is induced by a collective bootstrapping of the magnetic (exchange and/or dipolar) interactions as occurs in the tetragonal $LiTbF_4$ material [39]. In $Tb_2Ti_2O_7$, a priori, it is theoretically possible that there could be no moment on the Tb^{3+} site for a concentration x of Tb^{3+} less than some critical concentration x_c in $(Tb_xY_{1-x})_2Ti_2O_7$, as occurs in $LiTb_xY_{1-x}F_4$ [39]. This is an important issue. Indeed, one could imagine that for the highly-frustrated pyrochlore lattice, the collective development of a permanent ground-state moment would not give rise to homogeneous moments on the Tb^{3+} sites, but to a kind of "modulated moment structure". This idea is conceptually similar to what is found in the frustrated tetragonal $TbRu_2Ge_2$ material [40], but where for $Tb_2Ti_2O_7$ there might be instead a quantum-disordered state "intervening" between a trivial singlet ground state and a long-range ordered one, with the quantum-disordered state extending all the way to $x = 1$.

In the case where a permanent moment does exist on Tb^{3+} even in absence of interaction (i.e. the limit $x \to 0$ in $(Tb_xY_{1-x})_2Ti_2O_7$), the important issue is to determine the wavefunction decomposition of the ground state in terms of $|J, M_J\rangle$ states and the symmetry, Heisenberg or otherwise, of the resulting effective spin variable. The goal of such a programme is to construct a low-energy effective spin Hamiltonian in order to tackle theoretically why $Tb_2Ti_2O_7$ does not order at nonzero temperature. Consequently, it is very important to know in more details what the magnetic nature of the Tb^{3+} single-ion ground state in $Tb_2Ti_2O_7$ is.

The main purpose of this paper is to examine the mag-

netic nature of the Tb^{3+} ion in the $Tb_2Ti_2O_7$ pyrochlore in order to assess whether or not there is indeed a *permanent* moment at the Tb site as the temperature goes to zero, and determine the nature of this moment (e.g. level of effective spin anisotropy). We present in Section II experimental evidence, based on results from d.c. susceptibility, heat capacity and powder inelastic neutron studies that show there is a permanent moment at the Tb site, but that its approximate $5\mu_B$ value is less than the value of $9.4\mu_B$ estimated from the d.c. susceptibility measurements above 200K [36], or the $9.72\mu_B$ $^7F_6$ free ion value. To complement the experimental work, results from abinitio crystal field calculations that take into account covalent and electrostatic effects are presented in Section III and Appendix B. We discuss in Section IV the possibility that dipole-dipole interactions and extra perturbative exchange couplings beyond nearest-neighbor may be responsible for the lack of ordering in $Tb_2Ti_2O_7$.

II. EXPERIMENTAL METHOD & RESULTS

A. Sample Preparation

Samples of $Tb_2Ti_2O_7$ and $(Tb_{0.02}Y_{0.98})_2Ti_2O_7$ were prepared in the form of polycrystalline pellets by high temperature solid state reaction. Starting materials, Tb_2O_3, Y_2O_3 and TiO_2 were taken in stoichiometric proportions, mixed thoroughly, pressed into pellets and heated in an alumina crucible at 1400^oC for 12 hours in air. Tb_2O_3 was prepared by hydrogen reduction of Tb_4O_7. The powder x-ray diffraction patterns of the samples, obtained with a Guinier-Hagg camera, indicate that they are single phase with cubic unit cell constants, a_0, of $10.491\mathring{A}$ for $Tb_2Ti_2O_7$ and $10.104\mathring{A}$ for $(Tb_{0.02}Y_{0.98})_2Ti_2O_7$. The value for the concentrated sample is in excellent agreement with previous reports [41,42].

Some of this high quality polycrystalline material was then used as starting material for a successful single crystal growth using an optical floating zone image furnace. Details of the crystal growth are described elsewhere [43].

B. d.c. Magnetic Susceptibility Measurements

As a first step towards determining the magnetic nature of the electronic ground state of the Tb^{3+} cations in $Tb_2Ti_2O_7$, we have investigated the d.c. magnetic susceptibility of $Tb_2Ti_2O_7$ and $(Tb_{0.02}Y_{0.98})_2Ti_2O_7$. The d.c. magnetic susceptibility was measured using a SQUID magnetometer(Quantum Design, San Diego) in the temperature range 2-300 K. The inverse susceptibility, χ^{-1}, of $Tb_2Ti_2O_7$ measured at an applied field of 0.01 Tesla is shown in Fig. 2. A fit of the data to the Curie-Weiss (CW) law above 200 K gives an effective paramagnetic moment of $9.4\mu_B/Tb^{3+}$ and an effective (high-temperature) CW temperature, θ_{CW} = -19 K, which indicates the dominance of antiferromagnetic interactions (the Curie-Weiss fits are done above 200 K). Deviation from the Curie-Weiss law sets in at a rather high temperature, $T \sim$70 K. This is consistent with elastic neutron scattering results reported previously, which showed evidence for short range magnetic correlations at temperatures up to 50 K [36].

Recognizing that for Tb^{3+}, an $^7F_6$ even electron and non-S-state ion, there may be "crystal field" as well as exchange contributions to the experimentally determined θ_{CW}, a magnetically dilute sample, $(Tb_{0.02}Y_{0.98})_2Ti_2O_7$, was also studied. The data for this sample are shown in Fig. 3 along with a Curie-Weiss fit giving again a value close to the free ion value for the effective paramagnetic moment, $9.6\mu_B/Tb^{3+}$, and $\theta_{CW} \approx -6$ K. This finite value is in contrast to the essentially zero θ_{CW} value obtained for a similarly diluted sample of $Gd_2Ti_2O_7$ which contains the isotropic "spin only" $^8S_{7/2}$ Gd^{3+} ion [13], and therefore indicates that a significant crystal field contribution to θ_{CW} exists in the Tb^{3+}−based material. Thus, to a first approximation one can estimate that the portion of θ_{CW} for $Tb_2Ti_2O_7$ which can be attributed to magnetic *interactions* is
$\theta_{CW}\{Tb_2Ti_2O_7\}$ - $\theta_{CW}\{(Tb_{0.02}Y_{0.98})_2Ti_2O_7\} \sim$ -13 K, a value similar to the $\theta_{CW} \approx$ -10 K found for $Gd_2Ti_2O_7$ [13]. This approach can be made more rigorous by noting that in a high-temperature series expansion, one finds that the magnetic susceptibility is $\chi = C_1(1/T + C_2/T^2)$ where $C_2 \equiv \theta_{CW}$ can be "decomposed" as a simple sum of terms that are ascribed to exchange interactions, dipolar interactions and crystal-field terms (see Appendix A). Note also that, down to a temperature of $T = 2$ K, neither Fig. 2 nor Fig. 3 show any sign of a singlet ground state which would manifest itself as an approach to a constant susceptibility with decreasing temperature, as found in the single ground-state of the $Tm_2Ti_2O_7$ [25]. A more detailed analysis concerning this issue is presented in Section III.

While it is tempting to use the magnetic interaction contribution $(\theta_{CW} - \theta_{CW}^{cf}) \approx -13$ K, (with $\theta_{CW} \approx -19$ K and $\theta_{CW}^{cf} \approx -6$ K), to extract the approximate value of the nearest neighbor exchange, an estimate of the nearest neighbor dipole-dipole interaction for Tb^{3+} ions indicates an energy scale of about 1 K. Given the long range nature of dipolar forces, it becomes clear that the classical nearest neighbor exchange constant cannot be obtained from a measurement of the Curie-Weiss temperature until the effects of long range dipolar interactions on θ_{CW} have been understood. We find via a high temperature series expansion analysis of the long range dipolar contributions, θ_{CW}^{dip}, to the Curie-Weiss temperature (see Appendix A), that the estimated upper bound on θ_{CW}^{dip} is ferromagnetic and ~ 1.2 K (for needle-shaped powder crystallites), while the lower bound is antiferromagnetic and ~ -2.4 K (for slab-shaped powder crystallites). Consequently, we find that antiferromagnetic ex-

change interactions are predominantly responsible for the $(\theta_{\rm CW} - \theta_{\rm CW}^{\rm cf}) = -13$ K value determined above $T \gtrsim 200$ K, with a resulting $\theta_{\rm CW}^{\rm exchange} \in [-14.2, -10.6]$ K.

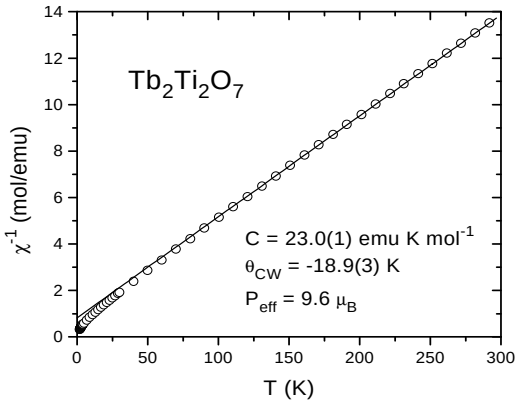

FIG. 2. Inverse molar susceptibility, $1/\chi$, of $Tb_2Ti_2O_7$ vs temperature.

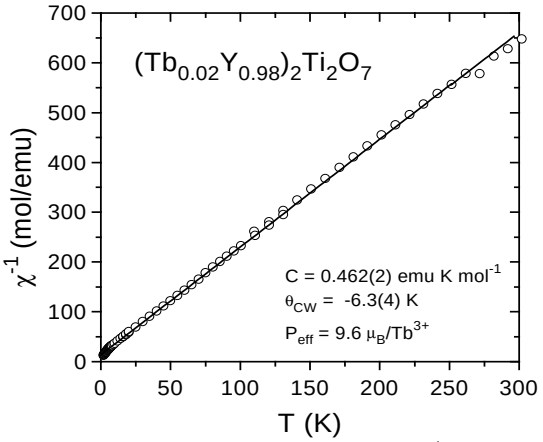

FIG. 3. Inverse molar susceptibility, $1/\chi$, of the diluted $(Tb_{0.02}Y_{0.98})_2Ti_2O_7$ material vs temperature.

C. Neutron Scattering Experiments

Inelastic neutron scattering allows us to determine with reasonable precision the values of the electronic energy levels of $Tb_2Ti_2O_7$. The inelastic neutron scattering measurements were carried out on a 50g sample of polycrystalline $Tb_2Ti_2O_7$, loaded in a sealed Al cell with a helium exchange gas present. The cell was mounted in a closed cycle helium refrigerator with a base temperature of 12 K. The sample was the same as used in reference [36]. Measurements were performed on the C5 triple axis spectrometer at the Chalk River Laboratories in constant scattered neutron energy mode. Two spectrometer configurations were employed, appropriate for relatively high and low energy resolution, respectively. Both configurations employed pyrolitic graphite (PG) as both monochromator and analyser. The low resolution measurements, appropriate for relatively high energy transfers, were performed using $\frac{E'}{h}$=3.52 THz (1THz=48 K), open-60-80-open collimation, and a PG filter in the scattered beam. The high resolution configuration used $\frac{E'}{h}$=1.2 THz, open-40-60-open collimation, and a cooled Be filter in the scattered beam. These results clearly indicate excitations at $E \approx 0.35$THz, 2.5THz and a broad neutron group centered at 3.5THz (corrsponding to 16.8 K, 120 K, and 168 K, respectively).

The low energy-resolution inelastic neutron scattering measurements at 12 K with $\frac{E'}{h}$=3.52 THz revealed the presence of two Q-independent modes with frequencies $\nu \sim 2.5$ and 3.5 THz. Representative neutron groups, as well as the dispersion relation for these two excitations are shown in the top panel of Fig. 4. These excitations are identified as being magnetic in origin due to their temperature and Q dependence. Their flat dispersion indicates that they are crystal electric field levels for Tb^{3+} in the environment appropriate for $Tb_2Ti_2O_7$.

The high energy-resolution inelastic neutron measurements at 12 K with $\frac{E'}{h}$=1.2 THz shows the presence of a low lying magnetic excitation near $\nu \sim 0.35$ THz. This mode is also dispersionless above a temperature of ~ 25 K, but partially softens in energy at the wavevector which characterizes the very short range spin correlations, which develop below 25 K. The development of this interesting dispersion has been described previously [36]. The dispersion of the low lying excitation is shown in the lower panel of Fig. 4. One can see that this partial softening of the excitation branch occurs only for the lowest lying mode. As we show in the next section, this is manifested in the heat capacity measurements as broad features that result of a broadening of the single-ion energy levels via these magnetic correlation effects.

These measurements place constraints on any calculations for the energy eigenstates of Tb^{3+} as they set both the energy spacing of the levels, and require that magnetic dipole matrix elements must connect the ground state with these levels in order that they be visible to the inelastic neutron scattering experiment. In particular, this indicates nonzero $\langle 0|J^+|1\rangle$, $\langle 0|J^-|1\rangle$, or $\langle 0|J^z|1\rangle$ matrix elements connecting the ground state, $|0\rangle$, and the first excited state, $|1\rangle$, at an energy ~ 0.35 THz $\approx$ 17 K above the ground state. In other words, there must be large $|J, M_J\rangle$ components in $|0\rangle$ and $|1\rangle$ where some of the M_J involved for the ground state and the excited state differ by 0, ± 1.

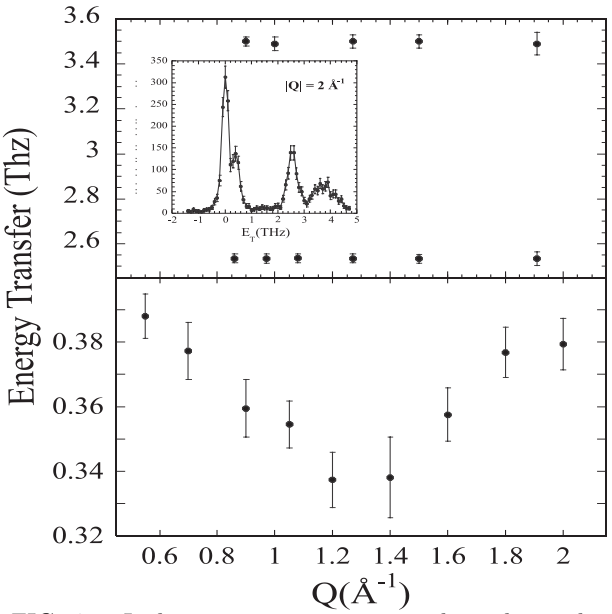

FIG. 4. Inelastic neutron scattering data obtained at a temperature $T = 12$ K. The inset of the top panel of Fig. 4 shows a transfer energy scan at $Q = 2\mathring{A}^{-1}$. Data showing representative neutron groups as well as the dispersion relation for these excitations at ~ 2.5 and 3.5 THz is shown in the top panel of Fig. 4. The dispersion of the low lying excitation is shown in the lower panel.

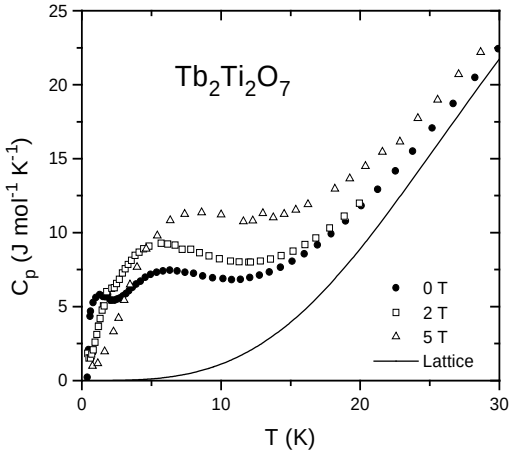

FIG. 5. Specific heat, C_p, of $Tb_2Ti_2O_7$ as function of temperature for the indicated magnetic fields of 0, 2 and 5 T. The solid line corresponds to the lattice specific heat of $Tb_2Ti_2O_7$, C_l, estimated from the measurements on the non-magnetic $Y_2Ti_2O_7$ that is isotructural to $Tb_2Ti_2O_7$ [52].

D. Specific Heat Measurements

Low-temperature specific-heat measurements on $Tb_2Ti_2O_7$ were performed using a thermal-relaxation microcalorimeter. The single crystal sample was mounted on a sapphire holder which was isolated from the bath by four copper-gold alloy wires. The relative precision and absolute accuracy of the calorimeter were confirmed by measuring copper and gold standards. In principle, specific heat-measurements on a dilute $(Tb_{0.02}Y_{0.98})_2Ti_2O_7$ sample would be useful. Unfortunately, this is not technically easily feasible as the magnetic contribution to the total specific heat would be too small to be determined accurately.

The total specific heat, C_p, of $Tb_2Ti_2O_7$ was measured from 0.4 K to 30 K at applied fields of 0, 2 and 5 T (see Fig. 5). The zero field data exhibits two broad peaks centered at about 1.5 K and 6 K. The data are in agreement with those of Ref. [27], above a temperature of 0.4 K. Hyperfine contributions to the specific heat become important below 0.4 K for Tb−based compounds, as found for example in the $Tb_2(GaSn)O_7$ pyrochlore [50,51], and this is presumably the reason for the sharp increase of $C_p(T)/T$ found in Fig. 4 of Ref. [27] below 0.5 K. The solid line in Fig. 5 corresponds to the estimated lattice heat capacity, C_l, for $Tb_2Ti_2O_7$, determined by scaling the heat capacity for $Y_2Ti_2O_7$, which is insulating, nonmagnetic, and is isotructural to $Tb_2Ti_2O_7$ [52].

The magnetic specific heat, C_m, obtained by subtracting C_l from C_p, is shown in Fig. 6 for the three applied fields. With the application of a 2 T field the magnitude of the lower temperature peak diminishes and moves to a slightly higher temperature. In contrast, the position of the second peak does not change but increases in magnitude as the lower temperature feature begins to overlap with it. At 5 T the low temperature feature disappears completely and the remaining peak is shifted to higher temperatures.

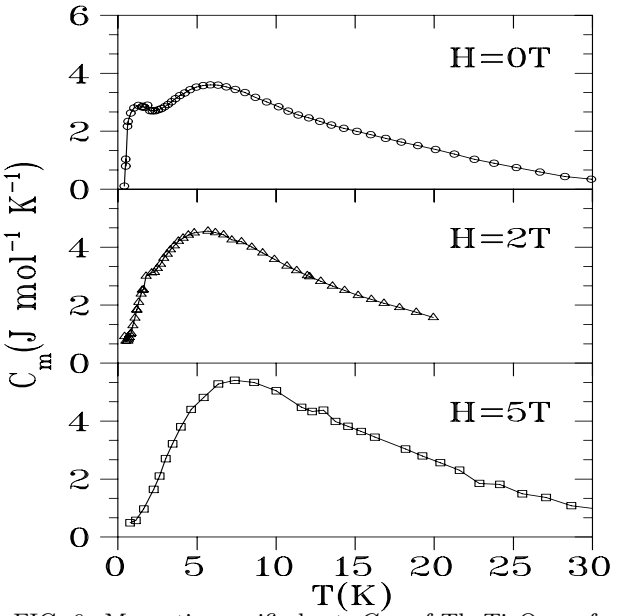

FIG. 6. Magnetic specific heat, C_m, of $Tb_2Ti_2O_7$ as function of temperature for the indicated magnetic fields of 0, 2 and 5 T. The solid lines are guides to the eye.

The crystal field calculations described in Section III and Appendix B (see Table 2) indicate a level scheme consisting of a ground state doublet with another doublet as the first excited state. Attempts to fit the C_m data to Schottky anomalies using a unique doublet−doublet level scheme for the Tb^{3+} ions and varying the ground state−excited state energy splitting failed, since important magnetic short-range correlations are present in this sytem, as discussed above in neutron scattering [36]. Consequently, we interpret the anomaly at $\sim$ 6 K as a remnant of the excited doublet that is "broadened" by exchange correlation fields, while the 1.5K anomaly is presumably due to these same correlation effects, but now acting on the single-ion ground state doublet. In other words, the build-up of short-range correlations in the low-temperature sector of the effective Hamiltonian for $Tb_2Ti_2O_7$ results in a specific heat anomaly at 1.5 K. This low-temperature anomaly at 1.5K that results from correlations is akin to the broad specific heat bump at $\approx$ 2 K found in $Gd_2Ti_2O_7$ [13]. However, $Gd_2Ti_2O_7$ is an $^8S_{7/2}$ spin-only ion, and there are no crystal field levels at high energy, nor are there correlation remnants of crystal field levels above the ground state such as those that cause the specific heat anomaly at 6 K in $Tb_2Ti_2O_7$. Another distinction between $Tb_2Ti_2O_7$ and $Gd_2Ti_2O_7$ is that the latter shows a very sharp specific heat anomaly at 0.9 K [13], and therefore presumably a transition to long range order at that temperature as suggested by recent neutron scattering experiments [14]. Down to 0.4 K, no such sharp specific heat anomaly is found in $Tb_2Ti_2O_7$. From the fit of the d.c. susceptibility and the crystal field calculations presented in Section III and Appendix B, good evidence is obtained that the magnetic moment in the ground state and the first excited state is $\sim$ 5 μ_B and $\sim$ 6 μ_B, respectively. Given a doublet-doublet energy gap of about 17 K, we can estimate the strength of the magnetic field where the separation between the doublets is equal to the magnetic field energy, and find a magnetic field of about 5 T. For an applied field of that strength, the ground state and excited states merge and are strongly mixed. This explains the disappearance of the low-temperature specific heat anomaly in Fig. 6 for a fuekd H = 5 T.

It is usual to estimate the magnetic entropy, $S_m(T)$, in a system by integrating $C_m(T)/T$ between the lowest temperature reached and the temperature, T, of interest. Although it is straightforward to integrate $C_m(T)/T$, the interpretation of the results for $Tb_2Ti_2O_7$ is difficult. The main reasons for this are:

- The hyperfine interaction is large for Tb^{3+} and the nuclear specific heat contribution becomes significant with respect to the magnetic contribution near 0.4K [50,51].
- There is a doublet crystal field excitation at an energy of approximately 17 K. Hence, one can hardly integrate $C_m(T)/T$ above 5 K without "already" embedding in the resulting entropy a contribution from excitations to the first excited doublet.
- From our neutron results and crystal field calculations presented in Appendix B, it is known that there are other levels at an energy $\sim 10^2$ K. Hence one cannot integrate $C_m(T)/T$ to obtain $S_m(T)$ up to a high enough temperature without having to consider the specific heat contribution from the states at $\sim O(10^2)$ K.
- By integrating $C_m(T)/T$ up to $\approx$ 30 K one enters a regime where the lattice contribution to the specific heat, $C_l(T)$, becomes sizeable (see Fig. 5). In that case the subtraction of $C_l(T)$ from the total $C_p(T)$ using rescaled results for the isostructural non-magnetic $Y_2Ti_2O_7$ leads to inherent uncertainties which increase dramatically above 10 K (see Fig. 5).

With these provisions in mind, we have determined $S_m(T)$ (see Fig. 7). We find that the recovered entropy, $S_m(T)$, at 15 K is already larger than that expected for a singlet−doublet energy level scheme, $S_m(15\text{K}) > \text{R}\ln(3)$. Since 15 K is much less than the excited states at $\sim$ 100 K, there should be little contribution to $S_m(15\text{K})$ coming from states at $T \gtrsim$ 100 K. Consequently, the results presented in this figure support further the picture that the two lowest energy levels in $Tb_2Ti_2O_7$ consists of two doublets. However, it is interesting to note that at a temperature of 30 K, the recovered entropy is not yet equal to Rln(4), the total entropy for two doublets. Either 30 K is not yet at high enough temperature to have recovered the full doublet−doublet entropy, or there exists macroscopic entropy in the ground state as occurs in $Dy_2Ti_2O_7$ [35].

For the four reasons mentioned above, it is difficult to make the discussion about the recovered entropy above 30 K in $Tb_2Ti_2O_7$ much more quantitative.

In summary the magnetic specific heat data are consistent with the inelastic neutron scattering results in that the two lowest-lying energy levels for Tb^{3+} in $Tb_2Ti_2O_7$ consist of two doublet energy levels separated by an excitation energy of $\sim 15 - 20$ K. As we will show in the next Section and Appendix B, our crystal field calculations strongly suggest that these two lowest lying levels are magnetic (Ising) doublets.

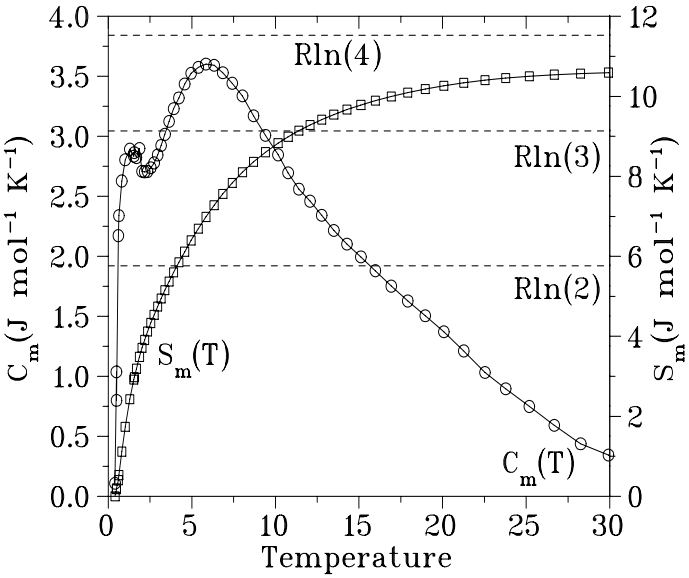

FIG. 7. Magnetic specific heat, $C_m(T)$, of $Tb_2Ti_2O_7$ in zero applied field (circles), and entropy, $S_m(T)$ (squares) are shown. The entropy values for two, three and four states are indicated by the horizontal dashed lines. R is the molar gas constant R= $N_0 k_B$ =8.3145 J mol^{-1} K^{-1}. The solid lines are guide to the eye.

III. SINGLE ION PROPERTIES

As discussed in the introduction, it is very important to determine whether the existence of a moment at the Tb^{3+} site in $Tb_2Ti_2O_7$ is intrinsic, or driven by magnetic interactions. Consequently, we have investigated in detail the problem of single-ion properties of Tb^{3+}, both theoretically and via d.c. susceptibility measurements, of $Tb_2Ti_2O_7$ and of the dilute $(Tb_{0.02}Y_{0.98})_2Ti_2O_7$ material where the Tb−Tb interactions should be negligible. The main conclusion from this investigation is that the Tb^{3+} cation does indeed carry an intrinsic moment inherent to its environment in $Tb_2Ti_2O_7$, and that moment is not due to a bootstrapping effect from interactions.

The results from inelastic neutron scattering and specific heat measurements presented in the previous section already provide some evidence for a doublet ground state and an excited doublet state at an energy of $\sim$ 17K. The purpose of this section is to investigate further from a theoretical point of view the question of the existence of a magnetic doublet ground state for Tb^{3+} in $Tb_2Ti_2O_7$. In short, both a simple point charge calculation and a more sophisticated ab-initio method confirm that a doublet−doublet scheme is the most likely low energy level structure for Tb^{3+}. We have constructed a van Vleck equation based on such a doublet−doublet scheme in order to parametrize the d.c. suceptibility of the dilute $(Tb_{0.02}Y_{0.98})_2Ti_2O_7$ sample, and to extract the value of the magnetic moment for both the ground state and excited state doublets. We find that experimental results for the d.c. susceptibility of $(Tb_{0.02}Y_{0.98})_2Ti_2O_7$ are in reasonably good agreement with the ab-initio calculations.

A. Crystal Field Effects

Experimental evidence of a doublet-doublet structure for the low temperature crystal field levels of Tb^{3+} in $Tb_2Ti_2O_7$ can be understood by considering the crystal field environment surrounding the ion. Pyrochlore oxides $A_2B_2O_7$ are described in space group $Fd\bar{3}m$ with A^{3+}, the trivalent rare earth in 16d, B^{4+}, the tetravalent transition metal ion, in 16c, O1 in 48e and O2 in 8b. The A or Tb^{3+} site in this case is coordinated to six O1 ions at about 2.5$\mathring{A}$ in the form of a puckered ring and to two O2 ions at a distance of 2.2$\mathring{A}$ in the form of a linear O2-Tb-O2 chain oriented normal to the mean plane of the O1 ring. The O2-Tb-O2 units are parallel to the (111) directions within the cubic unit cell. Overall, the local geometry at the Tb^{3+} site can be described as a severe trigonal compression along the body diagonal of a simple cube.

Based on symmetry considerations, the cubic plus axial distortion surrounding the Tb^{3+} ion may be expressed by a crystal field Hamiltonian of the general form

$$H^{\rm cf} = B_0^2 C_0^2 + B_0^4 C_0^4 + B_3^4 C_3^4 + B_0^6 C_0^6 + B_3^6 C_3^6 + B_6^6 C_6^6 \,, \qquad (3.1)$$

where the B_q^k's are yet to be determined crystal field parameters, and the C_q^k's are tensorial operators defined as $C_q^k = [4\pi/(2k+1)]^{1/2} Y_k^q$, where Y_q^k is a normalized spherical harmonic. In general, the B_q^k's represent an effective one-body potential which lifts the degeneracy of the angular momentum states in question. In practice, they may be determined experimentally by spectroscopic or thermodynamic probes, or theoretically within various levels of approximation.

In the simplest approximation of the crystal field interactions, one often uses the so-called point charge (PC) approximation where the crystal field is simply assumed to be caused by the Coulomb field of point charges situated at neighboring sites. In such a picture, the crystal

field eigenstates and eigenvalues have been determined for a number of rare earths by Lea *et al.* for systems with cubic symmetry (i.e. without trigonal distortion) [38]. For Tb^{3+}, the lowest three energy levels in a cubic environment are a Γ_3 singlet, a non-magnetic Γ_2 doublet and a $\Gamma_5^{(2)}$ triplet, with their precise ordering in terms of lowest energy states dependent upon variation of the point charge crystal field parameters [38]. In general, the addition of the trigonal distortion splits the $\Gamma_5^{(2)}$ triplet into a singlet and doublet, while the Γ_3 and Γ_2 states are preserved. Hence, we expect that the crystal field ground state of the Tb^{3+} ion in $Tb_2Ti_2O_7$ will be a competition between two doublets and two singlets.

Some notion regarding the difficulty of determining the precise ordering of these states and the size of their associated magnetic moments may be obtained by diagonalizing the crystal field Hamiltonian $H^{\rm cf}$ using Stevens' operator equivalents [53] of the C_q^k within a fixed J manifold [54], and by using the point charge approximation for the Coulomb effects of the surrounding oxygen ions. The resulting crystal field point charge Hamiltonian, $H_{\rm pc}^{\rm cf}$, with quantization axis along the appropriate $\langle 111 \rangle$ direction can be expressed as,

$$\begin{aligned} H_{\rm pc}^{\rm cf} &= \alpha_J \tilde{B}_2^0 (r^3 - 1) O_2^0 \\ &+ \beta_J \tilde{B}_4^0 \left[\frac{(27r^5 + 1)}{28} O_4^0 - 20\sqrt{2} O_4^3 \right] \\ &+ \gamma_J \tilde{B}_6^0 \left[\frac{(188 + 324r^7)}{512} O_6^0 + \frac{35\sqrt{2}}{4} O_6^3 + \frac{77}{8} O_6^6 \right], \quad (3.2) \end{aligned}$$

where $r = R_1/R_2$ and R_1, R_2 are the Tb-O distances for oxygen ions situated on the puckered ring and on the distortion axis respectively. The O_m^n represent crystal field operators as discussed by Hutchings [55], while α_J, β_J, and γ_J are the Steven's coefficients [53,55]. Trivalent Tb^{3+} is an $^7F_6$ ion and thus the fixed J manifold is $J = 6$ ($L = 3, S = 3, J = L + S = 6$) for the operator equivalent point charge calculation. The precise relationship between the point charge parameter set $\{\tilde{B}_q^k\}$ and the more general $\{B_q^k\}$ is discussed by Kassman [54].

Although a point charge estimation of the crystal field parameters is in most cases unreliable in predicting the actual crystal field level spacing of rare earth ions, we find that varying the point charge parameter set $\{\tilde{B}_q^k\}$ indicates that the ground state can be confirmed to be a competition between two singlets close in energy and two magnetic doublets, which are well separated from the other crystal field states. These levels are indeed the remnants of the Γ_2, Γ_3 and $\Gamma_5^{(2)}$ states of the cubic environment eluded to earlier.

In general, we find that in a large region of the crystal field parameter space, the two doublets form the lowest energy levels, although their precise ordering may change. Although the weight of each angular momentum component of a crystal field eigenstate varies with the values of the crystal field parameters, some other general features do emerge. In particular, one singlet contains only $|\pm 6\rangle$ and $|\pm 3\rangle$ states while the other is a combination of $|\pm 6\rangle, |\pm 3\rangle$ and $|0\rangle$. On the other hand both sets of doublets are *magnetic* (e.g they have a nonzero quantum expectation value of J^z), and also contain components of exclusively different J^z values (the J^z operator does not connect the ground state to the excited state). One doublet has large $|\pm 4\rangle$ and $|\pm 1\rangle$ components, while the other has large $|\pm 5\rangle$ and $|\pm 2\rangle$ components. Hence, the two doublets have M_J components that differ by ± 1, and a neutron spin-flip induced transition from one to the other is allowed, consistent with what is found in the inelastic neutron scattering results presented above.

We have confirmed these conclusions based on our point charge analysis by performing a more sophisticated first principles calculation that take into account both electrostatic and covalency effects as well as the intra atomic and configurational interactions. This approach, described in Appendix B, does not restrict the decomposition of the electronic energy levels into a *fixed* $|J, M_J\rangle$ manifold as is usually done using the Steven's operator equivalents, as discussed above. In the results presented in Appendix B, we find that the two lowest energy doublets have a leading $M_J = \pm 4$ and $M_J \pm 5$ components, respectively (close to 90% of the weight). Table 2 in Appendix B lists three very similar energy level structures given for slightly different constraints on the crystal field parameters. The theoretically determined energy levels (mean values: 0, 13, 60 and 83 cm^{-1}, that is 0, 19, 86, and 119 K, respectively, be compared with the experimental levels determined by inelastic neutron diffraction (0, 17, 115 and 168 K). The corresponding wavefunctions allow for a good estimate of the magnetic susceptibility of the diluted and concentrated compounds as shown by Table 3 and Figs. 2, 3, and 8.

From these results, a picture of the low temperature single-ion properties of Tb^{3+} can be deduced. Considering the structure of the eigenstates of the two lowest doublets, a calculation of their $g-$tensors indicates extremely strong Ising like anisotropy along the appropriate (111) axes (the axis formed by joining the two centers of the tetrahedra that the ion belongs to) for each Tb^{3+} ion at low temperatures. In summary, based on both point charge and ab inition calculations, we have strong evidence of a doublet$-$doublet scheme for Tb^{3+}, and a substantial single-ion anisotropy in $Tb_2Ti_2O_7$ [36] making the the Tb^{3+} moment effectively Ising$-$like for $T \lesssim O(10^1)$ K. The consequences of this result will be discussed in Section IV.

B. Susceptibility

The zero field susceptibility measurements of the powder Tb-diluted compound $(Tb_{0.02}Y_{0.98})_2Ti_2O_7$ shown in Fig. 3 enables us to gain a more concise understanding of the nature of the crystal field levels of Tb^{3+} in $Tb_2Ti_2O_7$,

and the single ion properties of Tb^{3+}. Indeed, the dilute concentration of Tb^{3+}ions in the system removes the effect of magnetic interactions and in principle leaves only crystal field contributions to the magnetic susceptibility. Having obtained strong evidence for a doublet− doublet scheme for the Tb^{3+} ions we now proceed further and analyse the d.c. magnetic susceptibility by constructing a phenomenological expression for the susceptibility based on a van Vleck equation for such a doublet− doublet energy level structure [72]. This allows us to extract the size of the magnetic moments of both doublets from experiment, as well as check for consistency with the conclusions based on our crystal field calculations of Appendix B.

Due to the powder nature of our $(Tb_{0.02}Y_{0.98})_2Ti_2O_7$ sample, the random orientation of the grains can lead to both parallel and transverse contributions to the susceptibility at first and second order. For the doublet-doublet structure at low temperature eluded to earlier, the van Vleck equation for the susceptibility has the general form

$$\chi = \frac{g^2\mu_B^2 N_{\rm Tb}}{3k_{\rm B}}\left(\frac{a/T + b + e^{-\Delta/T}(c/T - d)}{1 + e^{-\Delta/T}}\right), \quad (3.3)$$

where g is the Landé factor, equal to 3/2 for Tb^{3+}, μ_B is the Bohr magneton and $N_{\rm Tb} = 0.04N_0$, where N_0 is Avogadro's constant. The adjustable parameters a, b, c, d are defined through second order perturbation theory to be

$$a = \sum_{\alpha,n_0,m_0} |\langle n_0|J^\alpha|m_0\rangle|^2, \qquad c = \sum_{\alpha,n_1,m_1} |\langle n_1|J^\alpha|m_1\rangle|^2,$$
$$b = 2\sum_{\alpha,n_0,m_{i\neq 0}} \frac{|\langle n_0|J^\alpha|m_i\rangle|^2}{\Delta_{0,i}}, \quad d = 2\sum_{\alpha,n_1,m_{i\neq 1}} \frac{|\langle n_1|J^\alpha|m_i\rangle|^2}{\Delta_{1,i}},$$

where n_0, m_0 label states within the ground state doublet, n_1, m_1 label states in the excited doublet while the index i defines any state from the ith crystal field level. The Δ's represent crystal field energy level differences (in Kelvin) and $\alpha = x, y$ or z. The fitting parameters a and c are due to first order terms in perturbation theory while b and d are from second order terms and give rise to temperature independent van Vleck paramagnetism contributions to χ.

We have performed a least squares fit to the susceptibility data of $(Tb_{0.02}Y_{0.98})_2Ti_2O_7$ up to a temperature ~ 30 K, which is approximately where thermal contributions from a crystal field level at ~ 100 K become non-negligible. Because of the narrow energy spacing between the ground state and excited state doublet, *all four* adjustable parameters a, b, c, d are important in fitting the susceptibility data. Based on the crystal field calculations of the previous section, the specific heat analysis of the doublet-doublet gap in the concentrated $Tb_2Ti_2O_7$ sample, and the evidence of an anisotropy gap of ~ 17 K observed in inelastic neutron measurements on the same sample [36], we have carried out the fit of the low temperature behavior of the susceptibility using a doublet-doublet gap Δ ranging from $[12 \sim 24]$ K. We find that the goodness of fit is quite flat in this range for Δ. However the magnitude of the adjustable parameters do not deviate strongly and can be determined to a reasonable degree of accuracy over this interval. Using values of the gap outside of this interval yields a noticeably poorer goodness of fit. In Fig. 8, we show the fit to susceptibility data for the dilute $(Tb_{0.02}Y_{0.98})_2Ti_2O_7$ sample using an anisotropy gap of 17 K as well as the results for the ab-initio crystal field calculations.

We can interpret the fitted results for the susceptibility data by making use of our crystal field results and Eq. (3.3). Due to the strong Ising like nature of the $g-$tensors of the two theoretically calculated doublets, transverse terms such as $\langle n_i|J^{\pm}|m_i\rangle$ between two states *within* a doublet are negligible compared to $\langle n_i|J^z|n_i\rangle$. Thus, we expect that $a \simeq |\langle n_0|J^z|n_0\rangle|^2$ and $c \simeq |\langle n_1|J^z|n_1\rangle|^2$ and consequently, both the a and c terms represent permanent moment contributions to the susceptibility. For the same reason, the $g-$tensor characterizing the ground state is extremely anisotropic with essentially only a $g_\parallel$ component along the local $\langle 111\rangle$ direction with very little $g_\perp$ component. As a result, and this is the most important point of the paper:

At a temperature $T < O(10^1)$ K, Tb^{3+} ions can be considered to a very good approximation as (classical) Ising magnetic moments confined to point parallel or antiparallel to their local (111) *directions.*

Over the range mentioned above for the doublet-doublet gap Δ, we have found that the magnitude of the moment in the doublet ground state to be $5.10 \pm 0.3\mu_B$. Overall, we find that our best fit for the susceptibility data gives $a = 11.6 \pm .1, b = 1.53 \pm .04$ K^{-1}, $c = 15.7 \pm 4.0$ and $d = .71 \pm .05$ K^{-1}. The value of c gives a magnitude for the moment of the first excited doublet of $5.9 \pm .8\mu_B$.

Both fitted moments are compatible with the eigenstate structures of the doublets determined from the crystal field calculations presented in Appendix B. Additionally, the values of the paramagnetic terms b and d in the susceptibility are also consistent with our crystal field results. In particular, from the J^z components of our calculated low energy doublet and singlet eigenstates, there will be predominant contributions to b and d coming from transverse angular momentum matrix elements connecting the two doublets, as well as additional contributions involving transverse matrix elements between the doublets and the higher energy singlet states at $\gtrsim 100$ K. The doublet-doublet coupling will give equal (in magnitude) contributions to b and d while coupling to the singlets will give further positive contributions to b while reducing the value of d. This can be simply understood in terms of the signs of the denominators for each of these virtual excitation processes in our definitions of b and d.

In summary, we are able to successfully fit the $(Tb_{0.02}Y_{0.98})_2Ti_2O_7$ susceptibility measurements at low temperature using a doublet-doublet picture consistent with our crystal field calculations. We find reasonable

agreement in terms of calculated moments and paramagnetic contributions between that expected from theory and our fitted values. In particular, we find a permanent moment in the ground state of approximately $5.1\mu_B$. This moment is *intrinsic* to the Tb^{3+} ion and is *not* driven by exchange and/or dipolar interactions as occurs in $LiTbF_4$ [39]. This value is also compatible to what is estimated from the limiting low-temperature muon spin relaxation rate $1/T_1$ found in Ref. [36], assuming a dipole coupling between a positive muon μ^+ bounded to an oxygen at $\sim 2.5\mathring{A}$ away from a $\sim 5\mu_B$ Tb^{3+} moment (see Appendix C).

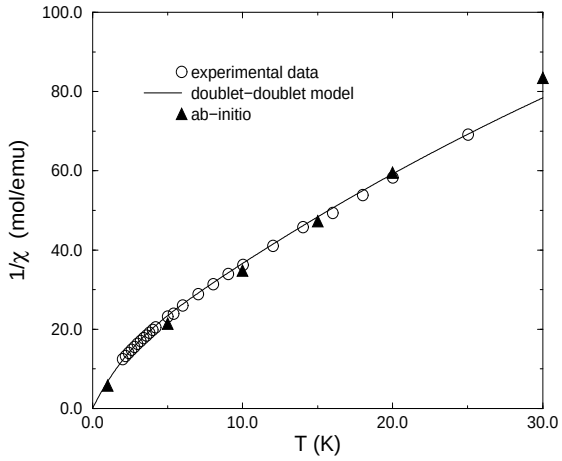

FIG. 8. Inverse susceptibility of $(Tb_{0.02}Y_{0.98})_2Ti_2O_7$. Circles indicate measured values while the solid line is a fit using Eq. (3.3) using a doublet-doublet gap of $\Delta = 18$ K. The solid triangles are the values obtained from the theoretical calculations of Appendix B.

IV. DISCUSSION

Combining together our results from d.c. susceptibility measurements, specific heat data, inelastic neutron scattering data, and crystal field calculations, the following picture emerges:

- The Tb^{3+} ion in $Tb_2Ti_2O_7$ carries a permanent magnetic moment of approximately $5\mu_B$. That moment is *intrinsic* to the Tb^{3+} ion and is not driven by magnetic correlation from exchange and/or dipolar interactions.
- The ground state is well described as an Ising doublet with extremely anisotropic $g-$tensor. In other words, the moments in the single-ion ground state are predominantly confined to point along the local (111) directions.
- The first excited state is at an energy of approximately 18 ± 1 K above the ground state, which is also characterized by a very anisotropic Ising-like $g-$tensor.
- Consequently, in the absence of interactions, the Tb^{3+} ions should be very well modeled below $T \lesssim O(10^1)$ K as *effective* classical Ising spins confined to point along the local (111) directions.

From d.c. susceptibility measurements at high temperature, we know that the magnetic interactions are predominantly antiferromagnetic, with $\theta_{\rm CW}^{\rm exchange} \approx -13$ K. Although the interactions are not small compared to the first excitation energy gap of 18 K, let us momentarily ignore the exchange coupling between the ground state and the excited doublet, and consider only the Ising-like ground state doublet. We then have a classical model with effective Ising spins pointing along their local (111) directions. In other words, spins that can only point either inward or outward on a tetrahedron.

Because of the open structure of the pyrochlore lattice, we expect that the nearest-neighbor exchange interactions predominate. If we make the further approximation that only nearest-neighbors contribute to the antiferromagnetic interactions, we arrive at a scenario where $Tb_2Ti_2O_7$ is effectively described by classical Ising spins pointing along the (111) directions and coupled via nearest-neighbor antiferromagnetic exchange. As discussed in Refs. [31,73,74], such a model is *not* frustrated. Indeed, if we pick one spin, and chose either an "in" or "out" orientation for it, then the three other spins on the same tetrahedron must also take the same "in" or "out" configuration to minimize the exchange interactions. Since the pyrochlore lattice can be described as an FCC lattice with a tetrahedron as the basis cell, either an "all in" or "all out" configuration repeats identically on all basis units; one refers to such a magnetically long-range ordered structure as a $Q = 0$ ground state [7,30].

The observation that $Tb_2Ti_2O_7$ remains paramagnetic down to at least 70 mK, while sustaining important short range magnetic correlations, is therefore very puzzling. We believe that the most plausible explanation is that the interactions in $Tb_2Ti_2O_7$ involve further than nearest-neighbor interactions, J_{nn}. The presence of these interactions, as well as the long-range dipolar interactions, possibly "reintroduce" large frustration in the spin Hamiltonian describing $Tb_2Ti_2O_7$, and conspire to destroy the "would-be" long-range Néel $Q = 0$ ground state, and give rise to a collective paramagnet−spin liquid, ground state.

V. CONCLUSION

In conclusion, we have presented results from d.c. susceptibility, specific heat, inelastic neutron scattering, and crystal field calculations for the pyrochlore lattice antiferromagnet $Tb_2Ti_2O_7$. We have obtained strong evidence that the Tb^{3+} magnetic moment on the 16d site at $T < 2$ K is *intrinsic* and is not induced by magnetic (exchange

and/or dipolar) interactions or correlation effects such as found in $LiTbF_4$ [39], and is of the order of $5\mu_B$. All evidence points towards a very strong Ising like anisotropy for the doublet ground state which forces the resulting classical Tb^{3+} Ising moments to point either parallel or antiparallel to their local $\langle 111 \rangle$ direction. For antiferromagnetic exchange interactions, such strong anisotropy largely removes all local ground state spin degeneracy, and should naively force the system to possess an Ising-like long range order ground state with all spins in or out on a tetrahedron basis cell. The reason for the failure of $Tb_2Ti_2O_7$ to order at a temperature $\sim [10^0 - 10^1]$ K set by the exchange part of the Curie-Weiss temperature remains unresolved at this time. The results presented here point towards the need to consider the role that exchange interactions beyond nearest-neighbor and dipolar interactions play in $Tb_2Ti_2O_7$.

VI. ACKNOWLEDGEMENTS

It is a pleasure to acknowledge contributions from B. Canals, S. Dunsiger, R. Kiefl and Z. Tun to these studies. We thank S. Bramwell, B. Ellman, P. Holdsworth, and D. Schmitt for very useful and stimulating discussions. This research was funded by NSERC of Canada via operating grants and also under the Collaborative Research Grant, *Geometrically Frustrated Magnetic Materials*. M.G. acknowledges the Research Corporation for a Research Innovation Award and a Cottrell Scholar Award, and the Province of Ontario for a Premier Research Excellence Award.

APPENDIX A: Dipole Contributions to $\theta_{\rm CW}$

The contribution from dipolar interactions to $\theta_{\rm CW}$ may be determined from a high temperature series expansion of the long range dipole-dipole Hamiltonian to first order in β. That is to say, given the additive property of crystal field effects, exchange and dipolar interactions to $\theta_{\rm CW}$, *i.e.* $\theta_{\rm CW} = \theta^{\rm cf}_{\rm CW} + \theta^{\rm ex}_{\rm CW} + \theta^{\rm dip}_{\rm CW}$, we may determine $\theta^{\rm dip}_{\rm CW}$ from an expansion of

$$\chi = \frac{g^2\mu_B^2}{kT}\langle \sum_{ij} J_i^z J_j^z \rangle_{H^{\rm dip}}$$

where z defines some global direction and we assume $T \gg \theta^{\rm cf}_{CW}$, *i.e.* isotropic spins. The angular brackets reflect an expectation value with respect to the dipole-dipole Hamiltonian $H^{\rm dip}$ defined by

$$H^{\rm dip} = \frac{1}{2} g^2\mu_B^2 \sum_{ij} \left(\frac{\mathbf{J}_i.\mathbf{J}_j}{|\mathbf{r}_{ij}|^3} - \frac{3(\mathbf{J}_i\cdot\mathbf{r}_{ij})(\mathbf{J}_j\cdot\mathbf{r}_{ij})}{|\mathbf{r}_{ij}|^5} \right).$$

To first order in β this yields

$$\chi = \frac{g^2\mu_B^2 N J(J+1)}{3kT}\left(1 - \frac{g^2\mu_B^2 J(J+1)}{3NkT}\Lambda\right),$$

and consequently that

$$\theta^{\rm dip}_{\rm CW} = -\frac{g^2\mu_B^2 J(J+1)}{3Nk}\Lambda \quad , \tag{A.1}$$

where

$$\Lambda = \sum_{ij} \frac{1}{|\mathbf{r}_{ij}|^3} - \frac{3|r^z_{ij}|^2}{|\mathbf{r}_{ij}|^5} \quad . \tag{A.2}$$

We see from the above analysis that the evaluation of $\theta^{\rm dip}_{\rm CW}$ involves the summation of a conditionally convergent series (a lattice sum), and thus special care must be taken in its evaluation. In general, it can be treated in a controlled manner by the use of a rapid convergence factor via the Ewald method [44,45]. Within the Ewald approach, the sum is split into two rapidly converging sums, one over the real space lattice and one in reciprocal space. Additionally, a surface (shape dependent) term also arises (which is interpreted as a demagnetization factor [45,46]).

Indeed, if we approximate the powder grains of the $(Tb_{0.02}Y_{0.98})_2Ti_2O_7$ as spherical, then the sum Eq. (A.2) is identically zero. This can be understood by imagining Eq. (A.2) as a sum over parallel (along the z axis) dipoles moments of magnitude unity. For a spherical object, it can be shown that such a sum must be identically zero for a system with cubic symmetry [47,48]. Accordingly there would be no dipolar contribution to the measured value of $\theta_{\rm CW}$ [49]. On the other hand, we do not expect that the geometry of the powder grains is in fact spherical, (additionally there is also the possibility of effects from inter-granular interactions). Therefore to gain an estimate on the *upper bound* of the dipolar contribution, we carry out the lattice sum Eq. (A.2) for an infinitely long cylinder (needle shape) along the z direction where surface effects are zero. This allows us to gain an approximate upper bound on the dipolar contribution as there are effectively no demagnetization effects. This calculation can be carried out rather simply by noting that for a spherical sample, Eq. (A.2), can be written using the Ewald method as [45]:

$$\Lambda_{\rm sphere} = \Lambda^{bulk} + \Lambda^{surface}_{\rm sphere} \quad , \tag{A.3}$$

where

$$\begin{aligned}\Lambda^{bulk} = \frac{M}{L^3}\sum_{i\neq j}\Bigg[&\sum_{\mathbf{n}} \frac{\alpha H(\alpha|\mathbf{R}_{ij}(\mathbf{n})|) + (2\alpha/\sqrt{\pi})e^{-\alpha^2|\mathbf{R}_{ij}(\mathbf{n})|^2}}{|\mathbf{R}_{ij}(\mathbf{n})|^2} \\ &- \sum_{\mathbf{n}} \frac{3\alpha|\mathbf{R}^z_{ij}(n^z)|^2 H(\alpha|\mathbf{R}_{ij}(\mathbf{n})|)e^{-\alpha^2|\mathbf{R}_{ij}(\mathbf{n})|^2}}{|\mathbf{R}_{ij}(\mathbf{n})|^4} \\ &- \sum_{\mathbf{n}} \frac{(2\alpha/\sqrt{\pi})|\mathbf{R}^z_{ij}(n^z)|^2(3+2\alpha^2|\mathbf{R}_{ij}(\mathbf{n})|^2)e^{-\alpha^2|\mathbf{R}_{ij}(\mathbf{n})|^2}}{|\mathbf{R}_{ij}(\mathbf{n})|^4} \\ &+ \sum_{\mathbf{n}\neq 0} 4\pi(n^z/|\mathbf{n}|)^2 e^{-\pi^2|\mathbf{n}|^2/\alpha^2} e^{2\pi i \mathbf{n}.\mathbf{r}_{ij}/L}\Bigg] \quad , \end{aligned} \tag{A.4}$$

$$\Lambda^{surface}_{\rm sphere} = \frac{M}{L^3}\sum_{i\neq j}\frac{4\pi}{3} \quad . \tag{A.5}$$

The $\mathbf{R}_{ij}(\mathbf{n}) = \mathbf{r}_{ij}/L + \mathbf{n}$, i,j label the dipole (Tb^{3+}) sites within the cubic unit cell, L is the length of the conventional cubic cell for $Tb_2Ti_2O_7$ and M is the number of cells in the sample. The function $H(y) = (2/y\sqrt{\pi})\int_y^\infty e^{-x^2}dx$ while $\mathbf{n} = (k,l,m)$ such that k,l,m are integers and α is suitably chosen to ensure rapid convergence of the summations over $\mathbf{n}$. Based on the previously mentioned result that Λ_{spher} should vanish for a spherical sample, this implies that the first four terms in the above expression, Λ^{bulk}, must sum to the opposite value of the last term ($\Lambda^{surface}_{\rm sphere}$, the surface term), and indeed we have verified that this is the case numerically. For an infinitely cylindrical sample, the surface term, $\Lambda^{surface}_{\rm cylinder} = 0$, and thus one finds

$$\begin{aligned}\Lambda_{\rm cylinder} &= \Lambda^{bulk} + \Lambda^{surface}_{\rm cylinder} \\ &= \Lambda^{bulk} \\ &= -\frac{M}{L^3}\sum_{i\neq j}\frac{4\pi}{3} \\ &\sim -1005\frac{M}{L^3} \quad . \end{aligned} \tag{A.6}$$

On the other hand, for a slab geometry, we have

$$\Lambda_{\rm slab} = \Lambda^{bulk} + \Lambda^{surface}_{\rm slab} \quad . \tag{A.7}$$

where

$$\Lambda^{surface}_{\rm slab} = \frac{M}{L^3}\sum_{i\neq j} 4\pi \quad ,$$

thus arriving at

$$\Lambda_{\rm slab} = \frac{M}{L^3}\sum_{i\neq j}\frac{8\pi}{3} \quad . \tag{A.8}$$

Combining Eqs.(A.1), (A.6) and (A.8), and using a cubic cell length of $L \sim 10.104$Å, [36] we arrive at upper and lower bounds for dipolar contributions to the Curie-Weiss temperature, namely $-2.4 \lesssim \theta^{\rm dip}_{\rm CW} \lesssim +1.2$ K.

APPENDIX B: Crystal Field Calculations

Our aim in this Appendix is to pursue in more details and using a more sophisticated (ab-initio) approach the calculations of the magnetic susceptibilites of $Tb_2Ti_2O_7$ and $(Tb_{0.02}Y_{0.98})_2Ti_2O_7$. To do so, we need to determine the electronic structure of the ground $^7F_6$ level of the Tb^{3+} ($4f^8$ configuration) in these two compounds, deduce the wavefunctions and from there infer the value of the magnetic moment of the ground state level. The determination of the $4f^8$ electronic configuration is obtained by diagonalizing the following Hamiltonian for a generic f^n configuration without making the fixed J manifold approximation used in Section III.A:

$$\begin{aligned}H(f^n) = \sum_k F^k(ff)f^k + \zeta(f)A_{so} + \alpha L(L+1) + \\ \beta C(\mathrm{G}_2) + \gamma C(\mathrm{R}_7) + \sum_{kq} B^k_q\, C^k_q \quad . \end{aligned} \tag{B.1}$$

Let us explain first what are the different terms in $H(f^n)$.

- The F^k's ($k = 2, 4, 6$) are the electrostatic integrals (Slater's parameters) which splits the $4f^n$ configurations into terms ^{2S+1}L where S is the total spin and L is the total orbital angular momentum. The f^k's are the associated two-electron operators [56].

- $\zeta(f)$ is the spin-orbit interaction integral which splits the terms into $^{2S+1}L_J$ levels. A_{so} is the associated one-electron spin-orbit operator [56].

- α, β and γ are parameters associated with effective two-body correction terms for inter-configuration interaction [57]. $C(\mathrm{G}_2)$ and $C(\mathrm{R}_7)$ are the Casimir's operators for groups G_2 and R_7. When $2 < n < 12$, there can be several terms ^{2S+1}L with the same S and L values in the f^n configuration. For instance there are three ^{5}G terms in $4f^8$ while there exists only one term ^{7}F. The states may differ by the way they are built from the parent configuration f^{n-1}. An additional classification of the states is therefore necessary. It is done according to the irreducible representations of the the groups G_2 and R_7 and bestows additional quantum numbers to the states.

- the B^k_q are the coefficients of the one-electron crystal field interaction which acts between $|^{2S+1}LJM_J\rangle$ sublevels. They can be theoretically predicted or extracted from fits of the energy levels (spectral lines) from experiments. In the point charge electrostatic model, their expression is :

  $$B^k_q = (4\pi/2k+1)^{1/2}\langle r^k\rangle\Sigma_j(Q_j/R_j^{k+1})Y_k^{q*}(\theta_j\phi_j)$$

  Where $\langle r^k\rangle$ is a $4f$ electron radial integral, Q_j is the point charge of ligand j, and R_j, θ_j, and ϕ_j, are

the polar coordinates of ligand j. The derivation of the B_q^k for the covalent interactions is much more involved [58]. The $C_q^k = (4\pi/2\mathrm{k}{+}1)^{1/2}[[\mathbf{Y}_k^q]]$, are the tensorial one-electron crystal field operators.

The evaluation of the matrix elements of *i)* the electrostatic interaction, *ii)* the spin-orbit interaction, *iii)* the free-ion configuration interaction, and *iv)* the crystal field interaction, between the states of the basis set chosen for the f^n configurations is necessary in order to determine the eigenvalues and eigenvectors of the latter. The matrix elements are calculated by the means of tensorial algebra [56]. Besides, if coupled $|^{2S+1}LJM_J\rangle$ states are chosen as the basis set, the one- or two-electron operators which are involved in the Hamiltonian cannot act directly on them. The calculation requires intermediary mathematical quantities known as reduced matrix elements which are tabulated for standard f^n configurations ([59]). Once evaluated, the complete matrix elements are multiplied by the associated parameters before diagonalization. The parameters are then determined by trial and error by successive diagonalizations and comparison of the eigenvalues with experimental energy levels. In the present case our main concern is the structure of the Tb^{3+} ground level, so that the only specific material dependent parameters which have to be determined before diagonalizing $H(f^n)$ are the B_q^k crystal-field interaction parameters. As already mentioned , the most convenient way to deduce the electronic structure of a rare earth ion in a solid compound, and hence determine the crystal-field parameters, is usually via analysis of its electronic spectrum by fitting the B_q^k to match the frequency of the observed transitions. The strongest lines are due to electronic transitions partly allowed by the mixing of the ground configuration with opposite parity configurations (Judd-Ofelt mechanism) [60,61]. However, in the case of pyrochlores, the site symmetry at the rare earth site is centrosymmetrical. The odd parity crystal field parameters vanish, the mixing of opposite parity configurations is impossible, hence no electric dipole transitions are detectable in the spectrum. Indeed, only the weak $^7F_1 \rightarrow {}^5D_0$ and $^7F_0 \rightarrow {}^5D_1$ magnetic dipole transitions were observed previously in the absorption spectra of the pyrochlore compounds $Eu_2Ti_2O_7$ and $Eu_2Sn_2O_7$ [62]. Hence a complete set of "phenomenological" crystal field parameters (CFP) cannot be determined from optical absorption or emission spectra. However, recent inelastic neutron scattering experiments have been able to give information on the lowest electronic levels of $Ho_2Ti_2O_7$ [27]. From these neutron results, some CFP's can be deduced. CFP's can also be calculated abinitio from the compound structure and the atomic data of the constituents. Therefore, in what follows, two approaches are used to determine the CFP's of $Tb_2Ti_2O_7$ and $(Tb_{0.02}Y_{0.98})_2Ti_2O_7$:

IA) A full ab-initio calculation of the CFP's utilizing the structural data of the compounds.

IB) The fit of the CFP's from the $Ho_2Ti_2O_7$ [27] and $Eu_2Ti_2O_7$ [62] data and a transposition to the $Tb_2Ti_2O_7$ and $(Tb_{0.02}Y_{0.98})_2Ti_2O_7$ compounds.

The next two steps for the calculations of the magnetic susceptibility are:

II) The calculation of the $4f^8$ electronic configuration utilizing plausible free ion parameters, and the fitted or calculated ab-initio values of the CFP's.

III) The calculation of the magnetic susceptibility of $Tb_2Ti_2O_7$ and $(Tb_{0.02}Y_{0.98})_2Ti_2O_7$ utilizing the wavefunctions derived from the previous step II.

These steps are detailed in the following :

IA) Ab-initio calculation of the CFPs

An ab-initio determination of the CFP's is obtained by adding an electrostatic and a covalent contribution along lines similar to the ones developed in Refs. [58,63] for oxygen ligands. The crystal structure, the ionic charges and the ionization energies of the ligands are used. In Ref. [64], experimental and predicted values of the parameters calculated by the "covalo-electrostatic" model were compared for ten compounds. The mean deviation between experimental and calculated values:

$$\Delta B^k/B^k = \left[\sum_{-k\le q\le k}(B^k_{qe}-B^k_{qc})^2 / \sum_{-k\le q\le k}(B^k_{qe})^2\right]^{1/2}$$
$$= [1 + 1/(S^k)^2 - 2\cos(R^k)/S^k]^{1/2}$$

where S^k and R^k are the scale and reliability factors listed in Table 7 of Reference [64]. $\Delta B^k/B^k$ is found to be equal to 52, 30 and 23% for $k = 2$, $k = 4$ and $k = 6$, respectively. Such is the uncertainty which can be expected from a "blind eyed" prediction of the CFP's of $Tb_2Ti_2O_7$.

As mentioned earlier, the space group of rare earth titanates with the pyrochlore structure is $Fd\bar{3}m$. The eight oxygen first neighbours form a distorted cubic polyhedron. Two oxygens occupy ideal positions on opposite summits of the cubic threefold axis. The three [[sides]] of the cube originating from each of these two summits are equally elongated. The a cubic lattice parameter is equal to 10.15 and 10.09 $\AA$, and x the positional parameter for the six displaced oxygens to 0.3 and 0.2968 for the dense and dilute compound respectively [42].

The site symmetry at the rare earth site is reduced from O_h (cubic) to D_{3d}. The remaining threefold order symmetry axis imposes for the crystal field parameters the condition $q = 0$, modulo 3, so that the non-zero even k CFP's are B_0^2, B_0^4, B_3^4, B_0^6, B_3^6 and B_6^6. The predicted

CFP values are reported in Table 1. The distances between the Tb^{3+} ion and the oxygens on the threefold axis is short (2.20 and 2.18 $\mathring{A}$ for the dense and the dilute compound, respectively) while the distances to the six peripheral oxygens are much larger (2.52 and 2.49 $\mathring{A}$, respectively). This explains why the "axial" B_0^k parameters are much larger than the "azimuthal" B_q^k's .

IB) Experimental determination of the CFPs.

The CFPs can be determined by fitting the energy levels of the f^n configuration either using spectroscopic or inelastic neutron scattering data from other pyrochlore compounds. Here, we can use the B_0^2 from spectroscopic data on $Eu_2Ti_2O_7$ [62] and the other B_q^k from neutron scattering data on $Ho_2Ti_2O_7$ [27].

- Determination of B_0^2 from spectroscopic data on $Eu_2Ti_2O_7$

  The $^7F_1 \rightarrow {}^5D_0$ and $^7F_0 \rightarrow {}^5D_1$ magnetic dipole transitions were observed previously in the electronic absorption spectrum of $Eu_2Ti_2O_7$ [62]. In the latter, the $^7F_1$ and $^5D_1$ splittings amount to 291 K and 51.9 K, respectively. A fit in $4f^6(Eu^{3+})$ yields $B_0^2 = 684$ K. The transposition to Tb^{3+} is made assuming the crystal field parameter is scaled by the ratio of radial integrals: $B_0^2(Tb^{3+}) = B_0^2(Eu^{3+}) \times \langle r^2 \rangle (Tb^{3+}) / \langle r^2 \rangle (Eu^{3+}) = B_0^2(Eu^{3+}) \times 0.91 =$ 622 K. This "experimental" value, listed in Table 1, and referred to as (a), has the same sign, but it is about half of the predicted value. As pointed out hereabove, the uncertainty on the calculated $k = 2$ parameters is large.

- CFP determination in $Ho_2Ti_2O_7$.

  Siddharthan et al. [27] recently reported results from ineleastic neutron scattering at low temperature in $Ho_2Ti_2O_7$. They determined the six lowest E irreducible representations of the $^5I_6$ ground state level. Utilizing their experimental values, we fitted the CFP's of Ho^{3+} while maintaining the ratio between CFP's with the same k value close to the theoretical ratio. The program ATOME was used for the refinement [65]. In this program, the basis set is composed of Slater determinants which makes unnecessary the use of tables of reduced matrix elements [65]. The evaluation of the matrix elements is straightforward, but the configuration cannot be truncated. Indeed, each eigenvector being a linear combination of a large number of Slater determinants, none of the latter can be omitted. As a consequence, all the 1001 states of $4f^{10}$ configuration are included in the diagonalization matrix. The basis is large (1001) but still tractable. The final mean deviation between experimental and calculated levels was equal to 7.8 K. The fitted CFP's are : $B_0^4 =$ 3173 K, $B_3^4 =$ -1459 K, $B_0^6 =$ 1343 K, $B_3^6 =$ 1292 Kand $B_6^6 =$ 609 K. As pointed out hereabove, the CFP's were then scaled according to the ratio between the radial integrals of Ho^{3+} and Tb^{3+} to give the experimental CFP's for $Tb_2Ti_2O_7$. Namely, $B_q^k(Tb^{3+}) = B_q^k(Ho^{3+}) \times \langle r^k \rangle (Tb^{3+}) / \langle r^k \rangle (Ho^{3+})$. These "experimental values" are are listed in Table 1, and referred to as (b). The experimental $k = 4$ and $k = 6$ CFP's are 1.7 and 1.9 times larger than the theoretical values which is somewhat unusual.

III) Calculation of $4f^8$ electronic configuration.

The calculation of the $4f^8$ electronic configuration is done by the means of program f^n [66] utilizing the Hamiltonian $H(f^n)$ in B.1 acting on coupled states $^{2S+1}L_J$. Contrary to program ATOME previously mentioned, program f^n can work on a truncated basis, which is necessary to resolve the $4f^8$configuration of $Tb^{3+}$with a large number of states (3003 states). The interaction matrix is built on a 387x387 basis set comprising the following $^{2S+1}$L terms of the Tb^{3+}($4f^8$) configuration: ^{7}F, ^{5}D(1,2,3), ^{5}F(1,2), ^{5}G(1,2,3), ^{3}P(1,2,3,4,5,6) and ^{1}S(1,2,3,4). The conjugate configuration of Tb^{3+} is that of Eu^{3+} with $4l+2-8 = 6$ electrons. The $4f^6$ (n=6) configuration of Eu^{3+} contains exactly the same number of basis states (e.g. [4l+2]!/[[4l+2-n]!n!] = 3003 states) as Tb^{3+}, the same terms, and the same levels. The interactions involving an odd number of electrons have a reverse sign in $4f^6$ and $4f^8$. For instance the $^{2S+1}L_J$ levels appear in a reverse order, and so do the crystal field sub-levels. In addition, the terms determined by the electrostatic interaction (two electron interaction) appear up in the same order for Eu^{3+} and Tb^{3+}.

For Eu^{3+} the above quoted basis had proved large enough to allow a simulation of the levels up to $^5D_2$ (30219 K) without drastic truncation effects [67]. The F^k's were assigned the Gd^{3+} values given in Ref. [68], that is 147289 K, [[102479 K]], and 55868 K for $k =$ 2, 4 and 6, respectively. α, β, γ were ascribed the Nd^{3+} values fitted in Ref. [69], that is 30.98 K, -1005.03 K, and 2510.48 K, respectively. The spin-orbit coupling constant $\zeta(f)$ was set equal to 2446.30 K which is a standard value for Tb^{3+} [70]. B_0^2 was assigned the transposed value quoted hereabove, and the other CFP's the values listed in Table 1 obtained after rescaling the B_q^k extracted from fits to the levels of Ho^{3+}. The diagonalization of the interaction matrix gives the energy levels and the corresponding leading eigenvectors listed in Table 2. The lowest levels are two doublets. Both states are rather Ising-like, with nearly exclusive (~ 0.95) $M_J = \pm 4$ and $M_J = \pm 5$ components. This is caused by the very "axial" crystal field parameters. In other words, the $M_J = \pm 4$ and $M_J = \pm 5$ carry, respectively, about 90% of the weight of the ground state and first excited state doublet wavefunctions.

III) Calculation of the magnetic susceptibility of $Tb_2Ti_2O_7$ and $(Tb_{0.02}Y_{0.98})_2Ti_2O_7$.

The d.c. magnetic susceptibility is by Van Vleck's formula [71,72] using the eigenvectors determined in the previous step.

$$\chi = \frac{N\mu_B^2}{\sum_i e^{-E_i^{(0)}/k_B T}} \left[\sum_i \frac{(\epsilon_i^{(1)})^2}{k_B T} - 2\epsilon_i^{(2)} \right] e^{-E_i^{(0)}/k_B T}$$

where N is the number of moles of Tb^{3+}, μ_B is the Bohr magneton, k_B is the Boltzmann constant, $E_i^{(0)}$ is the energy of the i^{th} level. Besides,

$$\epsilon_i^{(1)} = \langle \psi_i | \vec{L} + 2\vec{S} | \psi_i \rangle$$

$$\epsilon_i^{(2)} = \sum_{j \neq i} \frac{(\langle \psi_i | \vec{L} + 2\vec{S} | \psi_j \rangle)^2}{E_i^{(0)} - E_j^{(0)}}$$

The results as a function of the temperature are given in Table 3. The values for $\langle \mu(T) \rangle$ are very similar for the $Tb_2Ti_2O_7$ and $(Tb_{0.02}Y_{0.98})_2Ti_2O_7$ compounds. Therefore any large experimentally stated difference between the two compounds at low temperature cannot be accounted for by a difference in the individual characteristics of Tb^{3+} in the dense $Tb_2Ti_2O_7$ and the dilute $(Tb_{0.02}Y_{0.98})_2Ti_2O_7$.

TABLE 1

Empirical CFP's deduced by the covalo-electrostatic model for= $Tb_2Ti_2O_7$ and $(Tb_{0.02}Y_{0.98})_2Ti_2O_7$, and "experimental" CFP's for $Tb_2Ti_2O_7$. The latter are obtained using two approaches. (a) refers to the value of B_0^2 obtained by transposing to Tb^{3+} the value of B_0^2 determined from spectroscopic data of $Eu_2Ti_2O_7$. (b) refers to the values $B_q^{k\geq 4}$ obtained by transposing to Tb^{3+} the values of $B_q^{k\geq 4}$ determined from inelastic neutron data on $Eu_2Ti_2O_7$. All values in K. (PCEM = point charge electrostatic model.)

		B_0^2	B_0^4	B_3^4	B_0^6	B_3^6	B_6^6
	PCEM	471	708	-187			
$Tb_2Ti_2O_7$	Cov.	610	1599	-227	1261	314	482
	Total	**1081**	**2307**	**-414**	**1261**	**314**	**482**
	PCEM	407	731	-210			
$(Tb_{0.02}Y_{0.98})_2Ti_2O_7$	Cov.	609	1711	-288	1324	389	571
	Total	**1016**	**2442**	**-498**	**1324**	**389**	**571**
"Experimental"		**622**[a]	**3691**[b]	**-1698**[b]	**1731**[b]	**1665**[b]	**784**[b]

TABLE 2

Lowest energy levels (in K), irreducible representations in $(Tb_{0.02}Y_{0.98})_2Ti_2O_7$ and $Tb_2Ti_2O_7$, and leading compositions of the corresponding eigenvectors. Lines labelled (a) and (b) are for the *predicted* projections for the dilute $Tb_{0.02}Y_{0.98})_2Ti_2O_7$ and dense $Tb_2Ti_2O_7$, respectively, using the CFP's listed in Table 1. Lines labelled (x3) are for the predicted projections for the dense $Tb_2Ti_2O_7$ using the "experimental" CFP's listed in Table 1.

(E)	En	$^7F_6$, +/-4	$^7F_6$,+/-1	$^7F_6$,-/+5	$^5G_6(1)$, +/-4	$^5G_6(3)$, +/-4
(a)	0.	-0.97	+/-0.06	-/+0.06	+0.15	-0.14
(b)	0.	-0.97	+/-0.05	-/+0.06	+0.15	-0.14
(c)	0.	-0.95	+/-0.13	-/+0.13	+0.14	-0.13

(E)	En	$^7F_6$, +/-5	$^7F_6$,+/-2	$^7F_6$,-/+4	$^5G_6(1)$, +/-5	$^5G_6(3)$, +/-5
(a)	18.7	-0.96	+/-0.13	-/+0.07	+0.14	-0.13
(b)	15.9	-0.97	+/-0.11	-/+0.06	+0.14	-0.14
(c)	21.6	-0.92	+/-0.28	-/+0.14	+0.14	-0.13

(A2)	En	$^7F_6$,-3	$^7F_6$,3	$^7F_6$,-6	$^7F_6$,6	$^5G_6(1)$,-3	$^5G_6(3)$,3
(a)	86.5	+0.67	+0.67	+0.16	-0.16	-0.10	-0.10
(b)	87.9	+0.67	+0.67	+0.16	-0.16	-0.10	-0.10
(c)	85.0	+0.65	+0.65	+0.22	-0.22	-0.10	-0.10

(A1)	En	$^7F_6$,-3	$^7F_6$,3	$^7F_6$,-6	$^7F_6$,6	$^7F_6$,0
(a)	121.1	+0.66	-0.66	+0.21	+0.21	+0.07
(b)	118.2	+0.66	-0.66	+0.20	+0.20	+0.06
(c)	119.6	+0.64	-0.64	+0.25	+0.25	+0.11

TABLE 3

Ionic magnetic moment (in Bohr magnetons) and inverse molar magnetic susceptibility as a function of temperature.

T (K)	$\langle\mu\rangle$ (μ_B) $Tb_{0.02}Y_{0.98}Ti_2O_7$	$1/\chi$ (mole/emu) $Tb_{0.02}Y_{0.98}Ti_2O_7$	$1/\chi$ (mole/emu) $Tb_2Ti_2O_7$
1	5.90	5.8	0.11
5	6.84	21.4	0.41
10	7.58	34.8	0.67
15	7.97	47.3	0.92
20	8.20	59.5	1.17
30	8.47	83.5	1.65
300	9.22	706	14.09

† Present Address: NRC Canada, NPMR, Chalk River Laboratories, Building 459, Stn. 18, Chalk River, Ontario, K0J 1J0 CANADA

‡ Present Address: Department of Physics, The Ohio State University, Columbus, Ohio, 43210-1106

[1] G. Toulouse, Commun. Phys. **2**, 115 (1977).

[2] For recent reviews see: A.P. Ramirez, Annu. Rev. Mater. Sci., **24**, 453, (1994); *Magnetic Systems with Competing Interactions*, edited by H.T. Diep (World Scientific, Singapore, 1994); P. Schiffer and A.P. Ramirez, Comm. Cond. Mat. Phys., **18**, 21, (1996); M.J.P. Gingras, to appear in J. Phys. Cond. Matt. A.P. Ramirez, to appear in *Handbook of Magnetic Materials*.

[3] P. Chandra and P. Coleman, *New Outlooks and Old Dreams in Quantum Antiferromagnets*, Les Houches Summer School Lectures, North Holland, Amsterdam; Eds. Doucot and Zinn-Justin, 1991.

[4] P. Lecheminant, B. Bernu, C. Lhuillier, L. Pierre, and P. Sindzingre, Phys. Rev. B, **56**, 2521 (1997); Ch. Waldtmann, H.-U. Everts, B. Bernu, P. Sindzingre, P. Lecheminant, and L. Pierre, Eur. Phys. J. B **2**, 501-507 (1998) and references therein; F. Mila, Phys. Rev. Lett. **81**, 2356 (1998).

[5] B. Canals and C. Lacroix, Phys. Rev. Lett. **80**, 2933 (1998); ibid., to appear in Physical Review B.

[6] J. Villain, Z. Phys. B **33**, 31 (1979).

[7] J.N. Reimers, A.J. Berlinsky, and A.-C. Shi, Phys. Rev. B **43**, 865 (1991).

[8] R. Moessner and J. T. Chalker, Phys. Rev. Lett., **80**, 2929 (1998); R. Mossner and J.T. Chalker, Phys. Rev. B **58**, 12049 (1998).

[9] J.N. Reimers, Phys. Rev. B **45**, 7287 (1992).

[10] J.T. Chalker et al., Phys. Rev. Lett. **68**, 855 (1992).

[11] J.N. Reimers and A.J. Berlinsky, Phys. Rev. B **48**, 9539 (1993).

[12] G. Ferey et al., Rev. Chim. Miner. **23**, 474 (1986).

[13] N.P. Raju, M. Dion, M. J. P. Gingras, T.E. Mason and J.E. Greedan, Phys. Rev. B **59**, 14489 (1999).

[14] S.T. Bramwell, *Crystal and Magnetic Structure of Isotopic Gadolinium Titanate*, ISIS Experimental Report, Rutherford Appleton Laboratory. ISIS99 report #10394, (http://www.isis.rl.ac.uk).

[15] Kalvius, A. Martin, M. K. Krause, I. Halevy, J. Gal, W. Schdfer, G. Will, M. Hillberg, R. Wdppling Phys. Rev. B **53**, 9143 (1996).

[16] Strictly speaking, $ZnFe_2O_4$ and $ZnCr_2O_4$ are B-site spinels with no, or little inversion. However, the magnetic lattice of the B-site spinel is identical to the lattice of corner-sharing tetrahedra in pyrochlores [6].

[17] S.-H. Lee et al., cond-mat/9908433.

[18] S.R. Dunsiger et al., Phys. Rev. B **54**, 9019 (1996).

[19] M.J.P. Gingras, C.V. Stager, N.P. Raju, B.D. Gaulin and J.E. Greedan, Phys. Rev. Lett. **78**, 947 (1997).

[20] J.S. Gardner, B.D. Gaulin, S.-H. Lee, C. Broholm, N.P. Raju, and J.E. Greedan, Phys. Rev. Lett. **83**, 211 (1999).

[21] B. D. Gaulin,J. N. Reimers, T. E. Mason, J. E. Greedan, and Z. Tun, Phys. Rev. Lett. **69**, 3244 (1992).

[22] J.N. Reimers et al., Phys. Rev. B **43**, 3387 (1991).

[23] M.J. Harris et al., Phys. Rev. Lett. **73**, 189 (1994).

[24] J.E. Greedan, "Oxides with Trirutile and Pyrochlore Structures", in Landolt-Bornstein, New Series III, Vol. 27g, Springer-Verlag, Ed. H.P.J. Wijn, p. 105 (1992).

[25] M.P. Zinkin, M.J. Harris, Z. Tun, R.A. Cowley, and B.M. Wanklyn, J. Phys. Condens. Matt. **8**, 193 (1996).

[26] M.J. Harris, S. T. Bramwell, D. F. McMorrow, T. Zeiske, and K. W. Godfrey, Phys. Rev. Lett **79**, 2554 (1997).

[27] R. Siddharthan et al., Phys. Rev. Lett. **83**, 1854 (1999).

[28] In Ref. [27], Siddharthan et al. argued that the nearest-neighbor interaction is antiferromagnetic in $Ho_2Ti_2O_7$. This possibility is also discussed in two other recent papers [29,30]. In Ref. [27], Siddharthan et al. also considered the role dipolar effects in Ising pyrochlores. However, in their work, the dipole-dipole interaction was truncated beyond five nearest neighbor distances, and a sharp transition between paramagnetism and a partially ordered phase (where rapid freezing occurs) was observed for interaction parameters believed appropriate for $Ho_2Ti_2O_7$. From their simulation results, they argue that the $Ho_2Ti_2O_7$ material is not a spin ice, but shows partial ordering. However, it was recently argued that there is no experimental evidence for partial freezing in $Ho_2Ti_2O_7$ down to 50 mK [29]. As well, there is numerical evidence that the truncation of dipole-dipole interactions can be misleading, and introduce spurious features in various thermodynamic properties and, in particular, give rise to a transition to a partially ordered phase [29].

[29] B.C. den Hertog, M.J.P. Gingras, S.T. Bramwell and M.J. Harris, (unpublished).

[30] B.C. den Hertog and M.J.P. Gingras (unpublished).

[31] S.T. Bramwell and M.J. Harris, Phys. Condens. Matt. **10**, L215 (1998).

[32] M.J. Harris, S.T. Bramwell, P.C.W. Holdsworth, and J.D.M. Champion, Phys. Rev. Lett. **81**, 4496 (1998).

[33] M.J. Harris, Nature **399**, 311 (1999).

[34] L. Pauling, *The Nature of the Chemical Bond*, (Cornell Univ. Press, Ithaca, New York, 1945).

[35] A. P. Ramirez, A. Hayashi, R.J. Cava, R. Siddharthan and B.S. Shastry, Nature **399**, 333 (1999).

[36] J.S. Gardner, S.R. Dunsiger, B.D. Gaulin, M. J. P. Gingras, J.E. Greedan, R.F. Kiefl, M.D. Lumsden, W. A. MacFarlane, N.P. Raju, J. E. Sonier, I. Swainson, Z. Tun, Phys. Rev. Lett. **82**, 1012 (1999).

[37] S.R. Dunsiger et al., (unpublished).

[38] K.R. Lea, M.J.M. Leask, and W.P. Wolf, J. Phys. Chem. Solids **23**, 1381 (1962).

[39] P.E. Hansen, T. Johansson and R. Nevald, Phys. Rev. B **12**, 5315 (1975); R.W. Youngblood, G. Aeppli, J.D. Axe, J.A. Griffin, Phys. Rev. Lett. **49**, 1724 (1982).

[40] A. Garnier, D. Gignoux, D. Schmitt, and T. Shigeoka, Phys. Rev. B, **57**, 5235 (1998).

[41] L.H. Brixner, Inorg. Chem. **3**, 1065 (1964).

[42] O. Knop, F. Brisse and L. Castelliz, Can. J. Chem. **47**, 971 (1969).

[43] J.S.Gardner, B.D. Gaulin and D.McK. Paul, J. Crystal Growth **191**, 740 (1998).

[44] M. Born and K. Huang, *Dynamical Theory of Crystal Lattices*, p228 (Oxford University Press, London, 1968).
[45] S. W. de Leeuw, J. W. Perram and E. R. Smith, Proc. Roy. Soc. Lond. A. **373**, 27 (1980).
[46] M. W. Deem, J. M. Newsam and S. K. Sinha, J. Phys. Chem. **94**, 8356 (1990).
[47] H. A. Lorentz, *The Theory of Electrons* sec 117, (Teubner, Leipzig, 1909).
[48] A. Aharony and M. E. Fisher, Phys. Rev. B **8**, 33 23 (1973).
[49] Using the Ewald method, one finds that the surface term cancels the combined effect of both real and reciprocal space sums.
[50] H.W.J. Blöte, R.F. Wielinga, W.J. Huiskamp, Physica **43**, 549 (1969).
[51] The hyperfine interaction, A, for Tb−based compounds is $A \sim 300$ mK. See for example C.A. Catanese, A.T. Skjeltorp, H.E. Meissner, and W.P. Wolf, phys Rev.B **8**, 4223 (1973).
[52] R.P. Raju, E. Gmelin and R.K. Kremer, Phys Rev.B **46**, 5405 (1992).
[53] K. W. H. Stevens, Proc. Phys. Soc. (Lond.) **A65**, 209 (1952).
[54] A. J. Kassman, J. Chem. Phys. **53**, 4118 (1970).
[55] M. J. Hutchings, Solid State Phys. **16**, 227 (1964).
[56] B.R. Judd, *Operator Techniques in Atomic Spectroscopy*, Princeton University press, (1998).
[57] K. Rajnak and B.G. Wybourne, Phys. Rev. **132**, 280 (1963).
[58] D. Garcia and M. Faucher, J. Chem. Phys. **82**, 5554 (1985).
[59] C.W. Nielson and G.F. Koster, *Spectroscopic Coefficients for the p^n, d^n, and f^n configurations*, MIT Press (1963).
[60] B.R. Judd, Phys. Rev. **127**, 750 (1962).
[61] G.S. Ofelt, J. Chem. Phys. **37**, 511 (1962).
[62] M. Faucher and P. Caro, J. of Sol. St. Chem. **12**, 1 (1975).
[63] M. Faucher, D. Garcia and O.K. Moune, J. Lum. **51**, 341 (1992).
[64] D. Garcia and M. Faucher, *Handbook on the Chemistry and Physics of Rare Earths*, Eds K.A. Gschneidner and L. Eyring, **21**, 263 Elsevier 1995.
[65] D. Garcia, unpublished computer program "ATOME" (1988).
[66] M.D. Faucher, unpublished computer program "f^n".
[67] O.K. Moune and P. Caro, J. Less-Common Metals, **148**, 181 (1989).
[68] O.J. Sovers and T. Yoshioka, J. Chem. Phys. **51**, 5330 (1969).
[69] M. Chertanov, O.K. Moune, B. Piriou, J. Dexpert-Ghys, M. Faucher and M. Guittard, J. Lum. **59**, 231 (1994).
[70] W.T. Carnall, G.L. Goodman, K. Rajnak and R.S. Rana, *A Systematic Analysis of the Spectra of the Lanthanides Doped into Single Crystal LaF_3*, unpublished report ANL-88-8, Argonne National Laboratory, (February 1988).
[71] L. Beaury, *Influence du champ cristallin sur la susceptibilité paramagnétique du néodyme dans certains de ses composés*, Thèse de Doctorat, 3501, Paris-Sud, Orsay (1988).
[72] J. H. van Vleck, *Electric and Magnetic Susceptibilities*, (Oxford University Press, London, 1932).
[73] S. T. Bramwell, M. J. P. Gingras, J. N. Reimers, J. Appl. Phys. **75**, 5523 (1994).
[74] R. Moessner, Phys. Rev. B **57**, R5587 (1998)
[75] B.C. den Hertog, B. Canals, and M.J.P. Gingras (unpublished).